J Biomol NMR (2013) 55:225–230
DOI 10.1007/s10858-012-9703-9

NMR STRUCTURE NOTE

NMR structure note: a defective isoform and its activity-improved variant of a type III antifreeze protein from *Zoarces elongates Kner*

Hiroyuki Kumeta · Kenji Ogura · Yoshiyuki Nishimiya · Ai Miura · Fuyuhiko Inagaki · Sakae Tsuda

Received: 1 November 2012 / Accepted: 26 December 2012 / Published online: 4 January 2013

Biological context

Antifreeze proteins (AFPs) produced in various cold-adapted animals and plants can specifically bind to ice crystals and inhibit their growth (Fletcher et al. 2001; Graether and Sykes 2004). The ice-binding ability of AFPs depresses the freezing temperature (T_f) of water non-colligatively, which leads to the protection of cells and tissues from freezing. The level of T_f depression has been evaluated by measuring the T_f and melting temperature (T_m) for an ice crystal created in an aqueous solution of an AFP. The difference between these two temperatures is defined as the thermal hysteresis (TH), which is a measure of the AFP's ice-growth inhibition. AFPs also modify the shape of an ice crystal uniquely, hexagonal bipyramid for example, in the temperature range of TH. These two activities have been assumed to be common for all AFPs; however, it has recently been found that they are not always the rule for every species, such as the AFP type III (denoted AFPIII) found in fish (Takamichi et al. 2008).

Fish AFPIII is a globular protein made up of many short β-strands and one helical turn. AFPIII is generally produced in vivo as a mixture of quaternary-amino-ethyl (QAE)-Sephadex- and sulfopropyl (SP)-Sephadex-binding isoforms. These two isoforms possess different pIs and share approximately 50 % sequence identity. The Japanese notched-fin eelpout, *Zoarces elongates Kner*, produces 13 different AFPIII isoforms (denoted nfeAFP), which have been divided into six SP (nfeAFP1–6) and seven QAE (nfeAFP7–13) isoforms, and the latter was further divided into QAE1 (nfeAFP7–10) and QAE2 (nfeAFP11–13) isoforms (Nishimiya et al. 2005). Among them, only the QAE1 isoforms are fully active variants exhibiting both TH and ice-shaping activities, while the others only shape the ice morphology. The reason for such defective activity for the SP- and QAE2-isoforms is not well understood.

Recently, we found that alterations of the 9th, 19th, and 20th residues of a QAE2 isoform make them the same as their counterparts in the QAE1 isoform, leading to the successful conversion of the former into a QAE1-like fully active isoform (Garnham et al. 2012). That is, the QAE-2 isoform nfeAFP11 can only shape ice crystals, but has no TH activity, while its triple mutant nfeAFP11-V9Q/V19L/G20 V (denoted nfeAFP11-tri) perfectly exhibits both activities. These residues were thought to construct a "compound" ice-binding site (IBS) that consists of two adjacent flat surfaces inclined at an angle of approximately 150° to each other (Garnham et al. 2010). To determine if the triple mutations in nfeAFP11 led to changes in the structure of the IBS that could affect its ice-binding activity, the multidimensional NMR spectra of both nfeAFP11 and nfeAFP11-tri were examined. Special attention was paid to the surface-bound water molecules, for which the unique role of anchoring the IBS to ice lattice has been postulated (Garnham et al. 2011; Kondo et al. 2012).

The tertiary structures of AFPIII have been determined mostly for the QAE1-isoform HPLC12, which was identified in the ocean pout, *Macrozoarces Americanus*, by NMR and X-ray analysis. The currently available structural

H. Kumeta · K. Ogura · F. Inagaki
Faculty of Advanced Life Science, Department of Structural Biology, Hokkaido University, Kita21 Nishi11, Kita-ku, Sapporo 001-0021, Japan

Y. Nishimiya · A. Miura · S. Tsuda (✉)
Bioproduction Research Institute, National Institute of Advanced Industrial Science and Technology (AIST), Sapporo 062-8517, Japan
e-mail: s.tsuda@aist.go.jp

database for AFPIII includes NMR structures (Sönnichsen et al. 1996; Miura et al. 2001), X-ray structures (Graether et al. 1999; Antson et al. 2001), and a neutron structure (Howard et al. 2011). On the basis of these data, Howard et al. identified an ice-like geometry for four of the water molecules bound to a pocket of the IBS formed by Gln^{9}, Thr^{18}, Val^{20}, and Met^{21}, for which the anchoring role that leads to the AFP–ice interaction was assumed. In the present study, a set of two- and three-dimensional (2D and 3D) NMR spectra for the defective (nfeAFP11) and active (nfeAFP11-tri) isoforms of AFPIII were obtained. Then, the solution NMR structures were determined, and the locations of the surface water molecules in the IBS were examined through nuclear Overhauser effect spectroscopy (NOESY) experiments.

Methods

Escherichia coli JM105 cells were transformed with a pKK223–3UC-based expression plasmid that contains synthesized DNA encoding either nfeAFP11 or nfeAFP11-tri. Each transformant was cultured in M9 minimal media. Then, ^{15}N-labeled NH_4Cl was added to this media for the expression of ^{15}N-labeled proteins of nfeAFP11 and nfeAFP11-tri. Separately, both ^{15}N-labeled NH_4Cl and ^{13}C-labeled glucose were added to the media to obtain $^{13}C/^{15}N$-labeled proteins. The final yields of the ^{15}N-labeled proteins of nfeAFP11 and nfeAFP11-tri were 52.5 and 13.5 mg/L, and those of the $^{13}C/^{15}N$-labeled proteins were 47.3 and 19.4 mg/L, respectively. All of the proteins were dissolved in a 50 mM phosphate buffer (pH = 6.8) containing 25 mM KCl to prepare solutions with a final protein concentration of 2 mM.

All NMR experiments were carried out at 4 °C on a Varian Unity INOVA 600 spectrometer. Two- and three-dimensional (2D and 3D, respectively) NMR spectra were processed using NMRPipe (Delaglio et al. 1995) software, and the data analysis was performed with the help of the Sparky program (Goddard and Kneller 1997). The assignment of the ^{1}H-, ^{13}C-, and ^{15}N-resonances was carried out using the following set of spectra; [^{1}H-^{15}N] heteronuclear single quantum coherence (HSQC), [^{1}H-^{13}C] HSQC, HNCO, HN(CO)CA, HNCA, CBCA(CO)NH, C(CO)NH, HBHA(CO)NH, HC(C)H-TOCSY (total correlation spectroscopy). All chemical shift values were referenced to 4,4-dimethyl-4-silapentane-1-sulfonic acid (DSS) and determined with using the frequency ratios: ($^{15}N/^{1}H$) = 0.101329118, ($^{13}C/^{1}H$) = 0.251449519 (Wishart et al. 1995). The inter-proton distance restraints for the structural calculations were obtained from ^{13}C-edited NOESY–HSQC and ^{15}N-edited NOESY–HSQC spectra using a 75 ms mixing time. The restraints for the backbone phi and psi torsion angles were derived from the chemical shifts of the backbone atoms using the TALOS + program (Shen et al. 2009). The structure was calculated using the CYANA 2.1 software package (Güntert 2004). As an input for the final calculation of the 3D structures, a total of 2072 distances and 78 angle restraints were used for nfeAFP11, and 2124 distances and 75 angle restraints were used for nfeAFP11-tri (Table 1). At each stage, 100 structures were calculated using 30,000 steps of simulated annealing, and a final ensemble of 20 structures was selected on the basis of the CYANA target function values. The atomic coordinates have been deposited in the Protein Data Bank (PDB code: 2lx2 for nfeAFP11, 2lx3 for nfeAFP11-tri). The hydrogen–deuterium (H–D) exchange experiment was also performed using the $^{13}C/^{15}N$-labeled proteins of nfeAFP11 and nfeAFP11-tri. The HSQC spectra were recorded in every 40 min at 4 °C for 14 h after dissolving the lyophilized samples, which gave us information about hydrogen-bond formation of the amide groups.

Table 1 NMR structural statistics of nfeAFP11 and nfe11AFP-tri

	nfeAFP11	nfeAFP11-tri
Number of NMR restraints		
Total NOE restraints	2072	2124
Intra and sequential range ($\|i-j\| \leq 1$)	919	961
Medium range ($1 < \|i-j\| < 5$)	321	324
Long range ($\|i-j\| \geq 5$)	832	839
Number of dihedral angle restraints	78	75
Number of violations		
Distance > 0.2 (Å)	0	0
Angle > Î	0	0
Structural coordinate rmsd (Å) (residue range 1–65)		
Backbone atoms	0.11	0.12
All heavy atoms	0.34	0.37
Ramachandran plot		
Most favored regions	76.7 %	73.1 %
Additionally allowed regions	21.5 %	25.1 %
Generously allowed regions	1.9 %	1.7 %
Disallowed regions	0.0 %	0.1 %

Results and discussion

The NMR structures of nfeAFP11 and nfeAFP11-tri were successfully determined by employing heteronuclear 2D- and 3D-NMR spectroscopy. All sets of NMR spectra, including the ^{1}H-^{15}N HSQC (Fig. 1a), were well-dispersed for each protein sample, which enabled a full assignment of the ^{1}H-, ^{13}C-, and ^{15}N-resonances of the two proteins. It appeared that the HSQC peaks originating from 9th, 10th, 11th, 19th, and 20th residues of nfeAFP11 were shifted by the V9Q/V19L/G20V triple-mutation (Fig. 1b), while no appreciable change was detected for the other residues. The 20th residue showed the largest chemical shift change. For

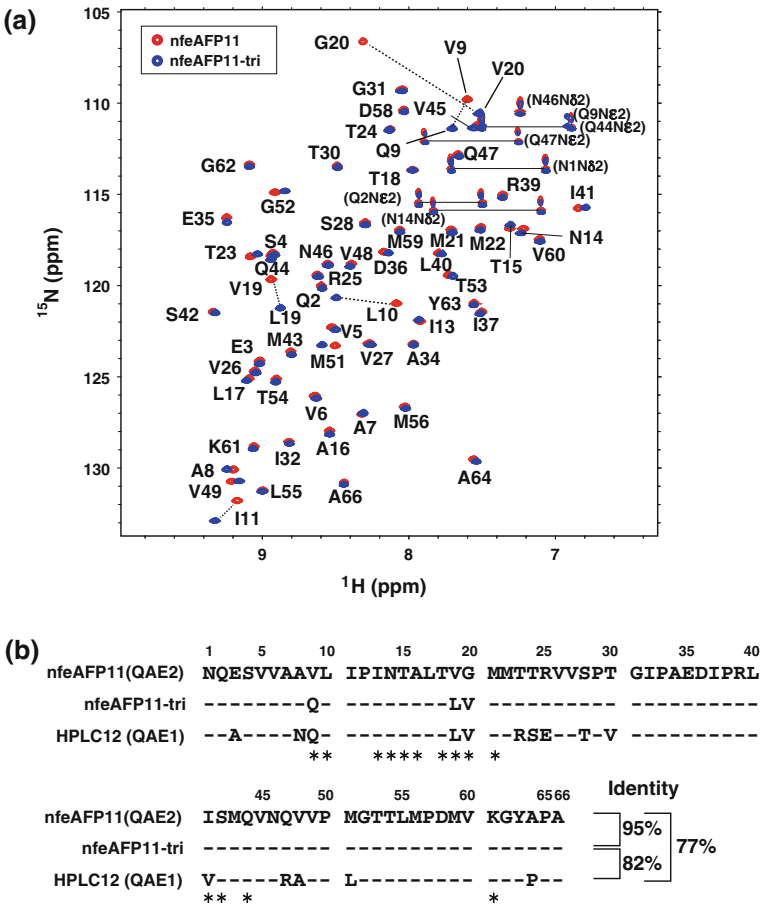

Fig. 1 Spectral assignment of a defective isoform of type III AFP (denoted nfeAFP11) and its activity-improved variant created by a V9Q/V19L/G20V triple-mutation (nfeAFP11-tri). (**a**) Superposition of [^{1}H-^{15}N] HSQC spectra of nfeAFP11 (*red*) and nfeAFP11-tri (*blue*) with the complete assignments. *Dotted lines* are drawn for some *peaks* to show their chemical shift change. (**b**) Sequence alignments of nfeAFP11, nfeAFP11-tri, and HPLC12. The *bars* show that the residues are identical to those of nfeAFP11. The residues involved in the ice-binding site (IBS) are indicated with *asterisks*

its NH-proton and nitrogen resonances, 0.53 and 7.95 ppm of higher-field shifts were evaluated, respectively, when it used the random coil shifts determined for Gly and Val (Schwarzinger et al. 2000). Hence these shifts were not merely caused by replacing Gly with Val.

Figure 2 shows the stereo views of the NMR-derived solution structures of (a) nfeAFP11 and (b) nfeAFP11-tri, each of which is an overlay of 20 superposed structures. The statistics for the calculated structures are listed in Table 1, and indicate that both satisfy the NMR-derived restraints and empirically allowed geometries for amino acids. The ribbon representations in Fig. 2c, d illustrate the stereo views of the lowest energy structures of nfeAFP11 and nfeAFP11-tri, respectively. The 9th to 19th residues construct one of two adjacent flat surfaces of the IBS, for which binding to the pyramidal plane of an ice crystal has been demonstrated for the HPLC12 isoform. The other surface binds to a primary prism plane when the protein's constituents are Thr^{18}, Leu^{19}, Val^{20}, and Ser^{42}. The nfeAFP11 contains Val^{19} and Gly^{20}, and lacks this second ability, while the triple mutation V9Q/V19L/G20 V converted nfeAFP11 into one that binds to both ice planes, leading to full TH activity (Garnham et al. 2012). However, in the present determined structures for nfeAFP11 and nfeAFP11-tri a root-mean-square deviation of only 0.37 Å in the backbone interatomic distances was evaluated for the 3–60th residues of the two proteins. In addition, the deviation between the crystal structure of HPLC12 (PDB code = 1HG7) and nfeAFP11 was 0.67 Å, and that between HPLC12 and nfeAFP11-tri was 0.69 Å. These values were similarly evaluated for currently available 24 PDB coordinates of single and double mutants of AFPIII. These results imply that there are no minor changes in the backbone structure of nfeAFP11 by the triple mutation, and that the basic structural coordinates between nfeAFP11, nfeAF11-tri, and HPLC12, which share 77–95 % of their sequence identities (Fig. 1b), are highly identical to one another.

Therefore, the activity improvement of nfeAFP11-tri might attributed to the change of surface complementarity that is limited to a region of the molecule. The surface complementarity or van der Waals force is one of the essential factors contributing to the ice-binding ability of AFPs. For example, in the 37-residue α-helical AFPI, an alanine-rich face including four equidistant threonines was assigned as the IBS, which is constructed with systematically spaced methyl-groups exhibiting a perfect match to the surface cavities of ice. Therefore, it may be assumed

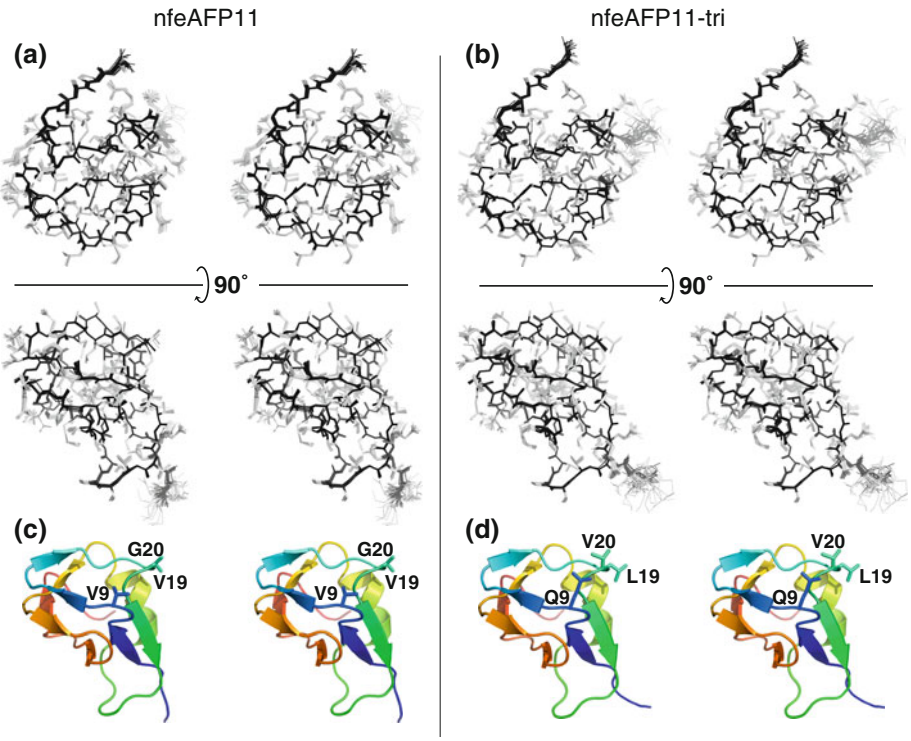

Fig. 2 Solution structures of nfeAFP11 and nfeAFP11-tri. Stereo views of the overlay of the ensemble of 20 final energy-minimized CYANA structures of (**a**) nfeAFP11 and (**b**) nfeAFP11-tri. In both, the main and side chains are shown in *black* and *gray*, respectively. Ribbon representations of the lowest energy structure of (**c**) nfeAFP11 and (**d**) nfeAFP11-tri. The 9th, 19th, and 20th residues that were mutated to enhance the activity, are represented by sticks and labeled for each model. The structures were created using PyMOL (http://www.pymol.org/)

that the triple mutations correct the irregularities in one of the surfaces of the IBS by introducing longer/larger hydrophobic side chains, thereby altering the 2nd surface such that a preferable match is made with the primary prism plane of ice.

In addition to the surface complementarity, an "anchored clathrate mechanism" was proposed to explain the AFP–ice interaction based on a structural study of AFPs with a β-helical motif (Liou et al. 2000; Garnham et al. 2011). This category of AFPs is mostly comprised of one amino acid sequence repeated in tandem, and the IBS consists of regularly aligned "trough-like" regions formed by ranks of threonyl side chains. The regularly spaced surface water molecules are located in this trough, and the distance between them closely matches that of the water molecules that form the ice prism/pyramidal plane. Therefore, it was assumed that the surface water molecules bound tightly to the IBS share the position of the water molecules in the ice lattice when the AFP attaches onto it, thereby working as anchored clathrate water molecules and strengthening the AFP–ice interaction.

Unlike the AFPs with a β-helical motif, AFPIII consists of no repetitive sequence and has no trough-like region on its surface. However, Howard et al. (2011) found an ice-like geometry of four water molecules bound to "a pocket region" in HPLC12 created by Gln^{9}, Thr^{18}, Val^{20}, and Met^{21}, where the OH-group of Thr^{18} was hydrogen bonded to the water cluster. The formation of this hydrogen bond was examined by ^{15}N- and ^{13}C-edited NOESY spectroscopy and the H–D exchange experiments.

Figure 3 depicts the expansion of data slice showing the side-chain resonance positions of Thr^{18} in (a) nfeAFP11 and (b) nfeAFP11-tri. Significantly, a signal originating from the γ-hydroxyl proton of Thr^{18} (Thr^{18}-HG1) at 5.10 ppm that is separate from the free water resonance (4.98 ppm), was observed only for nfeAFP11-tri. Such hydroxyl proton resonance is generally not observed due to a rapid exchange with the free water molecule, suggesting that Thr^{18}-HG1 forms a hydrogen bond with the surface water cluster only in nfeAFP11-tri. To obtain more precise knowledge about the hydrogen-bonding partner of Thr^{18}-HG1, we performed the H–D exchange experiments for nfeAFP11 and nfeAFP11-tri. In both samples, the HSQC resonance intensity of the following 19 residues were similarly decreased with time: Val^{9} (Gln^{9}), Leu^{10}, Ile^{13}, Asn^{14}, Thr^{15}, Met^{21}, Met^{22}, Gly^{31}, Ala^{34}, Asp^{36}, Arg^{39}, Ile^{41}, Ser^{42}, Asn^{46}, Gln^{47}, Val^{48}, Gly^{52}, Val^{60}, and Lys^{61}. Among them, amide group of Met^{21} is one of the candidates of the hydrogen-bonding partner of Thr^{18}-HG1, since Ala^{16}, Leu^{17}, Val^{19} (Leu^{19}), Gly^{20} (Val^{20}), and Met^{21} are only residues proximal to Thr^{18}-HG1 (< 5 Å) in the two protein structures. Significantly, the H–D exchange rate of Met^{21} was 36 times slowed in nfeAFP11-tri. Hence γ-hydroxyl proton of Thr^{18} may hydrogen bonded to amide group of Met^{21}. A strong NOE was also observed between the Thr^{18}-HG1 and the side chain methyl groups of Val^{20} for nfeAFP-tri. It should be noted that the V9Q-mutation significantly altered the growth speed of an ice crystal of nfeAFP11, and that Garnham et al. (2012) speculated an

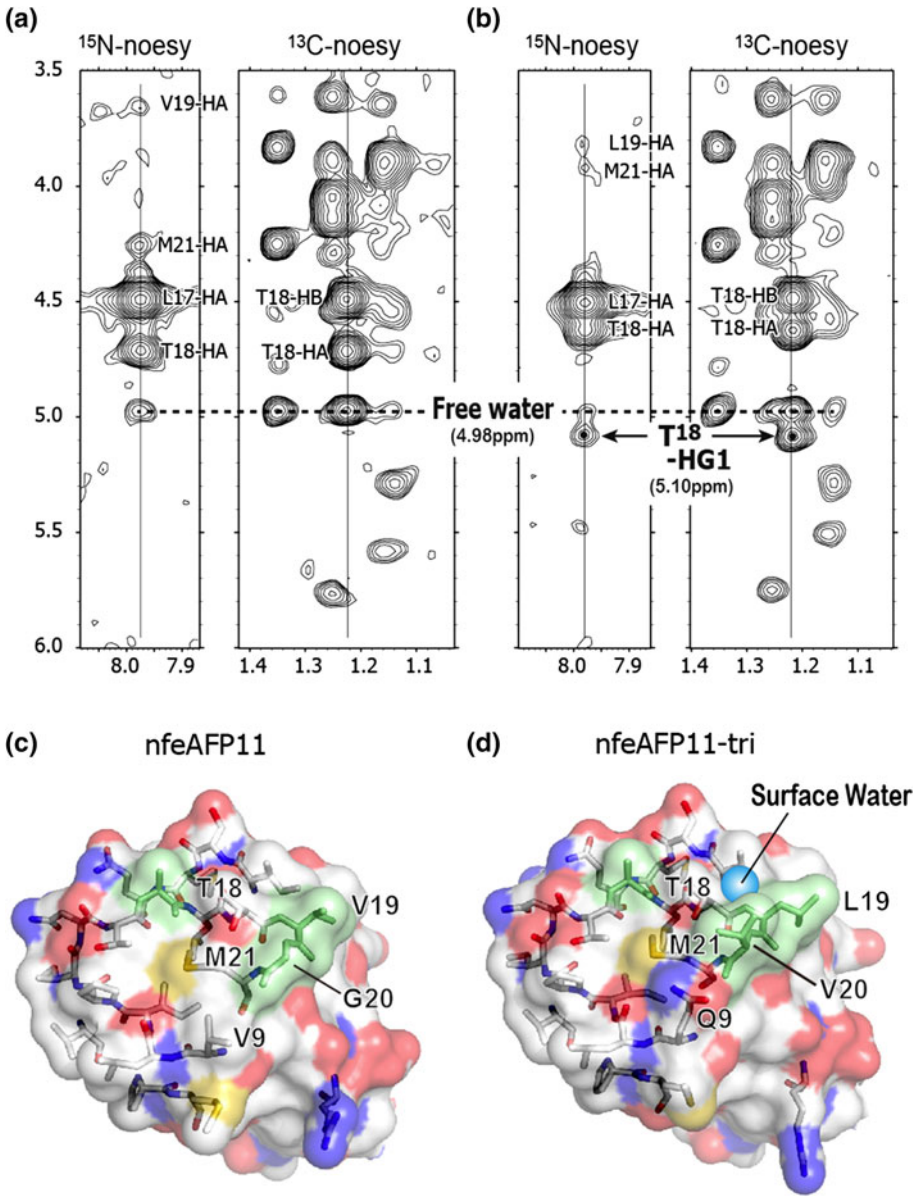

Fig. 3 NMR data suggesting the location of the surface-bound water of AFPs. Strips of the ^{15}N-edited and ^{13}C-edited NOESY spectra of (**a**) nfeAFP11 and (**b**) nfeAFP11-tri. The data show the *cross peaks* aligned to the Thr^{18}-HN position (^{15}N-NOESY) and those aligned to the Thr^{18}-CH$_3$ (HG2#) position (^{13}C-NOESY). The *peak* originating from the free water molecules is indicated by the *horizontal dashed line* (4.98 ppm). The *cross peak* from the γ-hydroxyl proton of Thr^{18} was only observed in (**b**). Illustrations showing the local environment around the Thr^{18} residue on the solution structures of (**c**) nfeAFP11 and (**d**) nfeAFP11-tri. The γ-hydroxyl proton of the Thr^{18} might be hydrogen-bonded to a surface-bound water trapped by the mutated residues in (**d**)

additional direct involvement of Gln^{9} in the hydrogen-bonded network of the waters. Overall, our current assumption is that the 9th and 18–21st residues of nfeAFP11 cannot form the surface pocket using the V^{9}, V^{19}, and G^{20} residues (Fig. 3c), while Q^{9}, L^{19}, and V^{20} residues of nfeAFP11-tri are capable of forming the pocket (Fig. 3d) similarly to HPLC12. Again the role of the surface pocket is to trap the ice-like water that anchor the AFP–ice interaction, for which Thr^{18}-HG1 may have a contribution in the case of nfeAFP11-tri.

Conclusion

We determined the NMR structures of a defective AFPIII isoform and its activity-improved variant. The structural constructions of the two isoforms were highly identical to one another; however, hydrogen bonding between Thr^{18} and a surface water molecule was suggested only for the active variant. Further NMR studies will provide more information about such waters that may control the activity of the AFPs.

Acknowledgments The authors thank Prof. Peter Davies at Queen's University for stimulating suggestions. This work was supported by a Grant-in-Aid for scientific research from the Japan Society for the Promotion of Science (JSPS) (No. 23310171) and from the Japan Bio-oriented Technology Research Advancement Institution (BRAIN).

References

Antson AA, Smith DJ, Roper DI, Lewis S, Caves LS, Verma CS, Buckley SL, Lillford PJ, Hubbard RE (2001) Understanding the

mechanism of ice binding by type III antifreeze proteins. J Mol Biol 305:875–889. doi:10.1006/jmbi.2000.4336

Delaglio F, Grzesiek S, Vuister GW, Zhu G, Pfeifer J, Bax A (1995) NMRPipe—a multidimensional spectral processing system based on unix pipes. J Biomol NMR 6:277–293. doi:10.1007/BF00197809

Fletcher GL, Hew CL, Davies PL (2001) Antifreeze proteins from teleost fishes. Ann Rev Physiol 63:327–357. doi:10.1146/annurev.physiol.63.1.359

Garnham CP, Natarajan A, Middleton AJ, Kuiper MJ, Braslavsky I, Davies PL (2010) Compound ice-binding site of an antifreeze protein revealed by mutagenesis and fluorescent tagging. Biochemistry 49:9063–9071. doi:10.1021/bi100516e

Garnham CP, Campbell RL, Davies PL (2011) Anchored clathrate waters bind antifreeze proteins to ice. Proc Natl Acad Sci USA 108:7363–7367. doi:10.1073/pnas.1100429108

Garnham CP, Nishimiya Y, Tsuda S, Davies PL (2012) Engineering a naturally inactive isoform of type III antifreeze protein into one that can stop the growth of ice. FEBS Lett 586:3876–3881. doi:10.1016/j.febslet.2012.09.017

Goddard TD, Kneller DG (1997) SPARKY 3, University of California, San Francisco http://www.cgl.ucsf.edu/home/sparky/

Graether SP, Sykes BD (2004) Cold survival in freeze-intolerant insects: the structure and function of β-helical antifreeze proteins. Eur J Biochem 271:3285–3296. doi:10.1111/j.1432-1033.2004.04256.x

Graether SP, DeLuca CI, Baardsnes J, Hill GA, Davies PL, Jia Z (1999) Quantitative and qualitative analysis of type III antifreeze protein structure and function. J Biol Chem 274:11842–11847. doi:10.1074/jbc.274.17.11842

Güntert P (2004) Automated NMR structure calculation with CYANA. Methods Mol Biol 278:353–378. doi:10.1385/1-59259-809-9:353

Howard EI, Blakeley MP, Haertlein M, Petit-Haertlein I, Mitschler A, Fisher SJ, Cousido-Siah A, Salvay AG, Popov A, Muller-Dieckmann C, Petrova T, Podjarny A (2011) Neutron structure of type-III antifreeze protein allows the reconstruction of AFP-ice interface. J Mol Recognit 24:724–732. doi:10.1002/jmr.1130

Kondo H, Hanada Y, Sugimoto H, Hoshino T, Garnham CP, Davies PL, Tsuda S (2012) Ice-binding site of snow mold fungus antifreeze protein deviates from structural regularity and high conservation. Proc Natl Acad Sci 109:9360–9365. doi:10.1073/pnas.1121607109

Liou YC, Tociij A, Davies PL, Jia Z (2000) Mimicry of ice structure by surface hydroxyls and water of a β-helix antifreeze protein. Nature 406:322–324. doi:10.1038/35018604

Miura K, Ohgiya S, Hoshino T, Nemoto N, Suetake T, Miura A, Spyracopoulos L, Kondo H, Tsuda S (2001) NMR Analysis of Type III Antifreeze Protein Intramolecular Dimer. Structural basis for enhanced activity. J Biol Chem 276:1304–1310. doi:10.1074/jbc.M007902200

Nishimiya Y, Sato R, Takamichi M, Miura A, Tsuda S (2005) Co-operative effect of the isoforms of type III antifreeze protein expressed in Notched-fin eelpout, *Zoarces elongatus Kner*. FEBS J 272:482–492. doi:10.1111/j.1742-4658.2004.04490.x

Schwarzinger S, Kroon GJA, Foss TR, Wright PE, Dyson HJ (2000) Random coil chemical shifts in acidic 8 M urea: implementation of random coil shift data in NMRView. J Biomol NMR 18:43–48. doi:10.1023/A:1008386816521

Shen Y, Delaglio F, Cornilescu G, Bax A (2009) TALOS+: a hybrid method for predicting protein torsion angle from NMR chemical shifts. J Biomol NMR 44:213–223. doi:10.1007/s10858-009-9333-z

Sönnichsen FD, DeLuca CI, Davies PL, Sykes BD (1996) Refined solution structure of type III antifreeze protein: hydrophobic groups may be involved the energetics of the protein-ice interaction. Structure 4:1325–1337. doi:10.1016/S0969-2126(96)00140-2

Takamichi M, Nishimiya Y, Miura A, Tsuda S (2008) Fully active QAE isoform confers thermal hysteresis activity on a defective SP isoform of type III antifreeze protein. FEBS J 276:1471–1479. doi:10.1111/j.1742-4658.2009.06887.x

Wishart DS, Bigam CG, Yao J, Abildgaard F, Dyson HJ, Oldfield E, Markley JL, Sykes BD (1995) ^{1}H, ^{13}C and ^{15}N chemical shift referencing in biomolecular NMR. J Biomol NMR 6:135–140. doi:10.1007/BF00211777